

EXTREME BLAZARS STUDIED WITH *FERMI*-LAT AND *SUZAKU*: 1ES 0347–121 AND BLAZAR CANDIDATE HESS J1943+213

Y. T. TANAKA¹, Ł. STAWARZ^{2,3}, J. FINKE⁴, C. C. CHEUNG⁴, C. D. DERMER⁴, J. KATAOKA⁵,
A. BAMBA⁶, G. DUBUS⁷, M. DE NAUROIS⁸, S. J. WAGNER⁹, Y. FUKAZAWA¹⁰, AND D. J. THOMPSON¹¹

Accepted by ApJ on 2014 April 11

ABSTRACT

We report on our study of high-energy properties of two peculiar TeV emitters: the “extreme blazar” 1ES 0347–121 and the “extreme blazar candidate” HESS J1943+213 located near the Galactic Plane. Both objects are characterized by quiescent synchrotron emission with flat spectra extending up to the hard X-ray range, and both were reported to be missing GeV counterparts in the *Fermi*-LAT 2-year Source Catalog. We analyze a 4.5 year accumulation of the *Fermi*-LAT data, resulting in the detection of 1ES 0347–121 in the GeV band, as well as in improved upper limits for HESS J1943+213. We also present the analysis results of newly acquired *Suzaku* data for HESS J1943+213. The X-ray spectrum is well represented by a single power law extending up to 25 keV with photon index 2.00 ± 0.02 and a moderate absorption in excess of the Galactic value, in agreement with previous X-ray observations. No short-term X-ray variability was found over the 80 ks duration of the *Suzaku* exposure. Under the blazar hypothesis, we modeled the spectral energy distributions of 1ES 0347–121 and HESS J1943+213, and derived constraints on the intergalactic magnetic field strength and source energetics. We conclude that although the classification of HESS J1943+213 has not yet been determined, the blazar hypothesis remains the most plausible option, since in particular the broad-band spectra of the two analyzed sources along with the source model parameters closely resemble each other, and the newly available *WISE* and *UKIDSS* data for HESS J1943+213 are consistent with the presence of an elliptical host at the distance of approximately ~ 600 Mpc.

Subject headings: radiation mechanisms: non-thermal — galaxies: active — galaxies: jets — gamma rays: galaxies — X-rays: galaxies — BL Lacertae objects: individual (HESS J1943+213, 1ES 0347–121)

1. INTRODUCTION

A rich population of very high energy (VHE; $E > 100$ GeV) γ -ray emitters has been discovered during a systematic scan of the Galactic plane with the High Energy Stereoscopic System (H.E.S.S.; Aharonian et al. 2005). The majority of these sources are Galactic in origin and those extended beyond the $\sim 0.1^\circ$ point-spread function (PSF) of the instrument include supernova remnants (SNRs), evolved pulsar wind nebulae (PWNe), or molecular clouds. H.E.S.S. sources in the Galactic plane that appear point-like are associated with the Galactic high-mass X-ray binaries (HMXBs), or young PWNe (e.g.,

the Crab Nebula). Outside of the Galactic plane, the unresolved γ -ray sources have been predominantly identified with active galactic nuclei (AGN). So far, more than 50 AGN, mostly blazars of the BL Lacertae type (hereafter BL Lacs), have been detected in the VHE range¹².

The unresolved, steady, and soft-spectrum (photon index $\Gamma_{\text{VHE}} = 3.1 \pm 0.5$) TeV source HESS J1943+213 was initially discovered in the Galactic plane scan data collected between 2005 and 2008, at the significance level of 7.9σ corresponding to a > 0.47 TeV photon flux of $\simeq 10^{-12}$ ph cm⁻² s⁻¹ (Abramowski et al. 2011). It is located within the $4.4'$ error circle of an unidentified hard X-ray *INTEGRAL* source IGR J19443+2117, which was also seen with *ROSAT*, *Chandra*, and *Swift* (Tomsick et al. 2009; Landi et al. 2009; Cusumano et al. 2010). Based on the gathered multi-wavelength data, Abramowski et al. (2011) argued in favor of the extragalactic (and in particular blazar) nature of the source (but see Gabányi et al. 2013, and the discussion below).

Blazars are AGN with relativistic jets pointed close to the Earth’s line of sight. The typical spectral energy distribution (SED) of a blazar is dominated by the non-thermal Doppler-boosted jet emission, and is characterized by two distinct components, or humps in the $\nu F_\nu - \nu$ representation: the low-energy one, commonly interpreted as due to synchrotron emission of ultra-relativistic jet electrons, peaking in the infrared-to-X-ray range, and the high-energy one peaking in the γ -ray regime, most widely believed to be due to inverse-Compton (IC) scattering of low-energy photons by the synchrotron-emitting electrons. The peak energy of

ytanaka@hep01.hepl.hiroshima-u.ac.jp

¹ Hiroshima Astrophysical Science Center, Hiroshima University, 1-3-1 Kagamiyama, Higashi-Hiroshima 739-8526, Japan

² Institute of Space and Astronautical Science, JAXA, 3-1-1 Yoshinodai, Chuo-ku, Sagami-hara, Kanagawa 252-5210, Japan

³ Astronomical Observatory, Jagiellonian University, ul. Orla 171, 30-244 Kraków, Poland

⁴ Space Science Division, Naval Research Laboratory, Washington, DC 20375-5352, USA

⁵ Research Institute for Science and Engineering, Waseda University, 3-4-1, Okubo, Shinjuku, Tokyo 169-8555, Japan

⁶ Department of Physics and Mathematics, Aoyama Gakuin University, 5-10-1 Fuchinobe, Chuo, Sagami-hara, Kanagawa 252-5258, Japan

⁷ UJF-Grenoble 1 / CNRS-INSU, Institut de Planétologie et d’Astrophysique de Grenoble (IPAG) UMR 5274, Grenoble, F-38041, France

⁸ Laboratoire Leprince-Ringuet, Ecole Polytechnique, CNRS/IN2P3, F-91128 Palaiseau, France

⁹ Landessternwarte, Universität Heidelberg, Königstuhl, D-69117 Heidelberg, Germany

¹⁰ Department of Physical Sciences, Hiroshima University, Higashi-Hiroshima, Hiroshima 739-8526, Japan

¹¹ NASA Goddard Space Flight Center, Greenbelt, MD 20771, USA

¹² <http://tevcat.uchicago.edu>

both spectral components was found to anti-correlate with the total radiative power, and also with the ‘Compton dominance’, i.e. the ratio of the IC and synchrotron luminosities (Fossati et al. 1998; Finke 2013), although the origins of these correlations are controversial (e.g., Ghisellini et al. 1998; Ghisellini & Tavecchio 2008; Giommi et al. 2012, 2013). High-frequency peaked BL Lacs (HBLs) occupy the lowest luminosity/highest frequency end of the blazar luminosity sequence, with the two spectral components peaking in X-rays (typically 0.1–1 keV) and in the VHE range (0.1–1 TeV), respectively.

As discussed in Abramowski et al. (2011), the broad-band spectral properties of HESS J1943+213 are consistent with the source being an example of the so-called ‘extreme HBL’ (see Costamante et al. 2001), only viewed through the Galactic disk and located at a minimum distance of ~ 600 Mpc (Abramowski et al. 2011). This distance limit would then set the X-ray luminosity of the source as $\gtrsim 10^{45}$ erg s $^{-1}$, which is relatively high for an HBL. Yet what is the most remarkable for this blazar candidate is its hard X-ray spectrum with no apparent cut-off up to 195 keV photon energies, as indicated by a long accumulation of the *Swift*-BAT data (see Baumgartner et al. 2013). This spectrum — if synchrotron in origin, as expected for an HBL — would then imply the action of persistent and extremely efficient energy dissipation processes, accelerating jet electrons up to the highest accessible energies. In this respect, HESS J1943+213 would in fact outshine the most extreme confirmed HBLs known to date, such as 1ES 0347–121 (Aharonian et al. 2007b) 1ES 0229+200 (Tavecchio et al. 2009; Kaufmann et al. 2011). We note that blazars are characterized by substantial broad-band variability at all accessible timescales, but the apparent lack of any flux changes in the case of HESS J1943+213, even though puzzling, does not strictly exclude the blazar hypothesis.

The class of extreme HBLs, which seems peculiar for its physical properties (particularly low magnetization but high bulk velocities of the emitting regions; see Tavecchio et al. 2010), may be relevant in the cosmological context, as it was argued that such objects can be utilized to derive lower limits on the intergalactic magnetic field (IGMF; e.g., D’Avezac et al. 2007; Neronov & Vovk 2010; Tavecchio et al. 2011; Dermer et al. 2011). That is because the $>$ TeV photons emitted from distant extreme HBLs are expected to efficiently pair-create on the extragalactic background light (EBL), leading to the formation of electromagnetic cascades evolving at cosmological scales and reprocessing the primary VHE blazar emission down to the GeV range. Since the resulting spectral shape of the reprocessed γ -ray continuum depends on the magnetization of the intergalactic medium, a precise characterization of the GeV spectra of extreme HBLs — which are typically very weak GeV emitters (Tavecchio et al. 2011) — are crucial in such attempts to constrain the IGMF.

In this paper we analyze the newly acquired *Suzaku* and *Fermi* Large Area Telescope (LAT) data for HESS J1943+213. Together with archival infrared data from the Wide-field Infrared Survey Explorer (*WISE*) and UKIRT Infrared Deep Sky Survey (*UKIDSS*) for the putative counterpart, we confront its broad-band spectral properties with those of the well-established extreme HBLs, including 1ES 0347–121 for which the *Fermi*-LAT and infrared data are similarly examined in detail. The data analysis and the analysis results are given in § 2 and § 3, respectively. Discussion regarding the nature of HESS J1943+213 in

the framework of the blazar scenario, along with the modeling of the broad-band spectra for both analyzed targets (including cascade components for different values of the IGMF), are described in § 4. Final conclusions are given in § 5. In the analysis we assume standard cosmology with $H_0 = 71$ km s $^{-1}$ Mpc $^{-1}$, $\Omega_m = 0.27$, and $\Omega_\Lambda = 0.73$.

2. DATA AND DATA REDUCTION

2.1. *HESS J1943+213*

2.1.1. *Fermi*-LAT Data

The LAT is a pair-production telescope onboard the *Fermi* satellite with large effective area (6500 cm 2 on axis for > 1 GeV photons) and large instantaneous field of view (2.4 sr at 1 GeV), and is sensitive to γ rays from 20 MeV to > 300 GeV (Atwood et al. 2009). Here, we analyzed *Fermi*-LAT data for both HESS J1943+213 and 1ES 0347–121 using the Fermi Science Tools version v9r27p1. The LAT data were accumulated from 2008 August 4 to 2013 February 08 and we selected 10–300 GeV SOURCE class events using `gtselect`. Regions of Interest (RoIs) were set to 10° circular regions centered at each source position. To eliminate Earth limb γ rays, the maximum zenith angle was set to 100° . Good-quality and science-configured LAT data were selected from standard all-sky data by using `gtmktime`. A 50° rocking angle cut is also applied. We performed unbinned likelihood analysis using `gtlike` and utilized the P7SOURCE_V6 instrument response functions. In the XML source model, we included 2FGL sources (Nolan et al. 2012) within a 10° circular region assuming their power-law spectra with free photon indices and normalizations. Spectral parameters of 2FGL sources within an annulus of 10 – 15° were fixed to the 2FGL values and included in the source model, together with `gal_2yearp7v6_v0.fits` and `iso_p7v6source.txt` which represent the Galactic and isotropic diffuse background emissions, respectively. Here, the photon index of the power-law scaling of the Galactic diffuse template is fixed to 0. Data points of the GeV spectra were calculated by repeating `gtlike` under assumption of a single power-law spectral shape in each energy range.¹³

2.1.2. Archival X-ray Data

HESS J1943+213 is located within the 4.4 arcmin error circle of the unidentified hard X-ray *INTEGRAL*-IBIS source IGR J19443+2117, with a centroid about 3.2 arcmin offset from the H.E.S.S. position. The soft X-ray counterpart to IGR J19443+2117 was detected by *Chandra* (CXOU J194356.2+211823; Tomsick et al. 2009) and *Swift* (SWIFT J1943.5+2120; Landi et al. 2009), with exposure times of 4.8 ks and 11 ks, respectively. The same X-ray source was also detected in the past by *ROSAT*-HRI (1RXH J194356.2+211824). The combined power-law fit to *Swift*-XRT and *INTEGRAL*-IBIS data returned the photon index of $\Gamma_X = 2.04 \pm 0.12$ with the energy fluxes $F_{2-10\text{keV}} = (1.83 \pm 0.04) \times 10^{-11}$ erg cm $^{-2}$ s $^{-1}$ and $F_{20-100\text{keV}} = (1.12 \pm 0.22) \times 10^{-11}$ erg cm $^{-2}$ s $^{-1}$ (Abramowski et al. 2011). Within the error of the cross-calibration constant between XRT and IBIS, $\simeq 0.60$, the IBIS data are in agreement with the XRT spectrum. The *Chandra* observations (performed two years earlier, in 2008) are consistent with the *Swift* results as well, with the derived energy flux

¹³ `likeSED.py`, available at <http://fermi.gsfc.nasa.gov/ssc/data/analysis/user/>

$F_{0.3-10\text{keV}} = (2.9^{+2.4}_{-0.5}) \times 10^{-11} \text{ erg cm}^{-2} \text{ s}^{-1}$ and $\Gamma_X = 1.83 \pm 0.11$. See Fig. 7 of Abramowski et al. (2011) for the consistency of the X-ray fluxes between *Swift* and *Chandra*. The *INTEGRAL*-SPI observations provided the upper limit for the source flux $F_{>100\text{keV}} < 2.6 \times 10^{-11} \text{ erg cm}^{-2} \text{ s}^{-1}$ (Bouchet et al. 2008). Finally, the hard X-ray counterpart of HESS J1943+213/ IGR J19443+2117 is also present in the 54-month Palermo *Swift*-BAT Catalog (PBC J1943.9+2118, $F_{14-150\text{keV}} = (2.2 \pm 0.7) \times 10^{-11} \text{ erg cm}^{-2} \text{ s}^{-1}$; Cusumano et al. 2010), and in the 70 month *Swift*-BAT catalog (Baumgartner et al. 2013). The BAT light curve seems to reveal some hints for flux changes over 70 months of monitoring¹⁴, but low photon statistics precludes a detailed analysis of the source variability.

A power-law model fit to the spectrum provided by Baumgartner et al. (2013) yielded $\Gamma_X = 2.12^{+0.25}_{-0.24}$ and the energy flux $F_{14-195\text{keV}} = 2.83^{+0.47}_{-0.44} \times 10^{-11} \text{ erg cm}^{-2} \text{ s}^{-1}$. There is no evidence for any high-energy cut-off in the BAT spectrum. Also, even though the IBIS source is weak, it appears steady with no signs of any large-amplitude variability. The hydrogen column densities derived by means of modeling the *Chandra* and *Swift* spectra were $N_H \simeq (1.89^{+0.25}_{-0.22}) \times 10^{22} \text{ cm}^{-2}$ (Tomsick et al. 2009) and $(1.37^{+0.12}_{-0.13}) \times 10^{22} \text{ cm}^{-2}$ (Landi et al. 2009), respectively.¹⁵ In spite of this column density being in excess of the expected Galactic one in the direction of the source based on the H I mapping (see § 3.1 below), no conclusive evidence for the intrinsic absorption in the X-ray spectrum of HESS J1943+213 was presented in the past.

2.1.3. New *Suzaku* Observation

We observed HESS J1943+213 with the *Suzaku* X-ray satellite (Mitsuda et al. 2007) on 2011 November 10–11 (Obs ID 706007010). We analyzed the data taken with both X-ray CCD cameras onboard, namely the X-ray Imaging Spectrometer (XIS; Koyama et al. 2007) and Hard X-ray Detector (HXD; Takahashi et al. 2007; Kokubun et al. 2007). Currently, three CCDs are working well, two of which are front-illuminated (XIS0 and XIS3) and the other one is back-illuminated (XIS1). The HXD consists of a Si semiconductor detector (PIN) and the GSO scintillator, sensitive to hard X-rays in the ranges of ~ 10 –50 keV and ~ 50 –600 keV, respectively. Here we did not analyze the GSO data because the relatively small flux of the targeted source does not allow us to detect hard X-rays above ~ 50 keV over the high background.

We used the XIS data processing script version 2.7.16.31 and followed the screening criteria described in *The Suzaku Data Reduction Guide*¹⁶. Events with GRADE 0, 2, 3, 4 and 6 were utilized in the data reduction procedure, and flickering pixels were removed by using `cleansis`. We selected good-time intervals by applying `SAA_HXD==0 && T_SAA_HXD>436 && ELV>5 && DYE_ELV>20 && ANG_DIST<1.5 && S0_DTRATE<3 && AOCU_HK_CNT3_NML_P==1`. After the event screening, the net exposure was 38.9 ks. In the analysis we used the HEADAS software version 6.12 and calibration database (CALDB) version released on 2012 Feb 11.

¹⁴ http://swift.gsfc.nasa.gov/results/bs70mon/SWIFT_J1943.5p2120

¹⁵ It is unclear why the *Swift*-XRT 11 ks observation provided much smaller uncertainty when compared to the *Chandra* 4.8 ks observation, taking into account the fact that *Chandra* ACIS-I has about four times larger effective area with respect to *Swift*-XRT at 1 keV (see Figure 1 in Tundo et al. 2012).

¹⁶ <http://heasarc.nasa.gov/docs/suzaku/analysis/abc/>

2.1.4. Lower Frequencies

There is only one radio source in the NVSS catalog within the error circle of HESS J1943+213, namely NVSS J194356+211826, offset by 14.7 arcsec from the H.E.S.S. source position and 3.5 arcsec from the *Chandra* source position. This radio source (1.4 GHz flux density of 0.103 Jy) has been detected in various survey programs and dedicated exposures between 327 and 4850 MHz; no evidence for flux variations over the 12-year time span of the collected radio data was found (Abramowski et al. 2011). Recent high-resolution data taken with the European VLBI Network (EVN) also revealed a compact radio source, and the low brightness temperature is claimed to be an argument against the blazar origin for this object (Gabányi et al. 2013).

A faint unidentified near-infrared counterpart of HESS J1943+213 was also found in 2MASS data in the *K* band, 2MASS J19435624+2118233, well within the small *Chandra* error circle; at smaller wavelengths (2MASS *J* and *H* bands, as well as *Swift*-UVOT *V* band), only upper limits for the source flux were found (Abramowski et al. 2011). We examined the subsequently available all-sky mid-infrared (MIR) data provided by *WISE* satellite (Wright et al. 2010) in four MIR bands, W1, W2, W3, and W4, centered on wavelengths around 3.4, 4.6, 12, and 22 μm , respectively. The PSF of the telescope corresponds to a Gaussian of about 6.1, 6.8, 7.4, and 12 arcsec in W1–W4 respectively, sampled at 2.8, 2.8, 2.8 and 5.6 arcsec/pix. With nominal 5σ point source sensitivities of ~ 0.08 , 0.1, 1 and 6 mJy in the four bands, this survey is orders of magnitude more sensitive than previous infrared all sky surveys¹⁷. The MIR emitter, WISE J194356.25+211823.2, coinciding with HESS J1943+213, is detected at 3.4 μm , 4.6 μm , and 12 μm wavelengths, with the observed fluxes of 1.88 ± 0.19 mJy, 1.67 ± 0.14 mJy, and 1.36 ± 0.27 mJy, respectively, and is not detected at 22 μm . Using the Schlegel et al. (1998) coefficients in adjacent bands, we can also estimate extinction corrected flux densities of 3.1 mJy (3.4 μm) and 1.9 mJy (4.6 μm); extinction is negligible at 12 μm . The 2MASS source is also catalogued in the *UKIDSS*-DR6 Galactic plane survey (Lucas et al. 2008) as UGPS J194356.23+211823.3, with observed *J* = 16.448 ± 0.010 , *H* = 15.187 ± 0.006 , and *K* = 14.174 ± 0.006 mag. Using the Schlegel et al. (1998) extinction corrections adopted in Abramowski et al. (2011), these correspond to the extinction-corrected fluxes of 4.18 ± 0.04 mJy (1.25 μm), 3.71 ± 0.02 mJy (1.65 μm), and 3.60 ± 0.02 mJy (2.21 μm), respectively. New near-infrared data for HESS J1943+213 will be presented in the forthcoming paper by (Peter et al. 2014).

2.2. 1ES 0347–121

The *Fermi*-LAT data selection and analysis for 1ES 0347–121 are the same as in the case of HESS J1943+213 (see § 2.1.1), except for the 1–300 GeV energy range considered. The reason why we decreased the lower energy threshold to 1 GeV is that 1ES 0347–121 is clearly detected in 10–300 GeV SOURCE class data. At lower frequencies, in addition to the archival *Swift*-UVOT and XRT, and ATOM (host galaxy-subtracted) data discussed in Aharonian et al. (2007b), we also include the newly updated *Swift*-BAT spectrum of the source (Baumgartner et al. 2013), and the most recent infrared measurements summarized

¹⁷ <http://wise2.ipac.caltech.edu/docs/release/allsky>

as follows: 1ES 0347–121 is detected in the *WISE* data at $3.4\ \mu\text{m}$, $4.6\ \mu\text{m}$, and $12\ \mu\text{m}$ wavelengths, yielding the observed fluxes of $0.64 \pm 0.02\ \text{mJy}$, $0.57 \pm 0.02\ \text{mJy}$, and $0.40 \pm 0.11\ \text{mJy}$, respectively, with negligible extinction in these bands; the extinction-corrected 2MASS fluxes for the source are $0.69 \pm 0.06\ \text{mJy}$ ($1.25\ \mu\text{m}$), $0.61 \pm 0.07\ \text{mJy}$ ($1.65\ \mu\text{m}$), and $0.93 \pm 0.09\ \text{mJy}$ ($2.17\ \mu\text{m}$).

3. RESULTS

3.1. X-ray Spectrum of HESS J1943+213

The *Suzaku*-XIS0+XIS3 combined image and light curves (in the 0.5–2.0 and 2.0–8.0 keV bands) of HESS J1943+213 are shown in Figures 1 and 2, respectively. No significant variability or modulation was seen over the entire 80 ks *Suzaku* pointing (40 ks net exposure). Since the hard X-ray signal detected with HXD/PIN was not very strong, the resulting light curve of the source above 10 keV was partly affected by statistical and systematic fluctuations, and as such is rather inconclusive. We also did not find any source extension beyond the XIS PSF of $\simeq 1.5\ \text{arcmin}$.

Figure 3 presents the simultaneous X-ray spectrum of the target within the 0.5–25 keV range (combined *Suzaku*-XIS and HXD/PIN data). The spectrum is well represented by a single power-law model (reduced $\chi^2_{\nu}/\text{d.o.f} = 1.11/847$) with photon index $\Gamma = 2.00 \pm 0.02$, absorbed by the hydrogen column density of $N_{\text{H}} = (1.38 \pm 0.03) \times 10^{22}\ \text{cm}^{-2}$, in agreement with the one emerging from the previous *Swift* observations, but in excess over the Galactic value of $8.37 \times 10^{21}\ \text{cm}^{-2}$ estimated based on the Galactic H I Leiden/Argentine/Bonn (LAB) Survey¹⁸ (Kalberla et al. 2005). We also applied an unabsorbed broken power-law model to the *Suzaku* spectrum of HESS J1943+213 and rejected it because of a much larger reduced chi-square value of 1.21 with respect to the single absorbed power-law model. The unabsorbed 2–10 keV flux of the source reads as $(1.85^{+0.07}_{-0.06}) \times 10^{-11}\ \text{erg cm}^{-2}\ \text{s}^{-1}$, again in remarkable agreement with the previous *Swift*-XRT observations (Abramowski et al. 2011), indicating that HESS J1943+213 is a truly steady X-ray emitter.

In order to investigate in more detail the issue of the excess absorption in the X-ray spectrum of HESS J1943+213, we have modeled the acquired *Suzaku* data with the SYNCHROTRON code developed and implemented in XSPEC by Ushio et al. (2009, 2010). In this “parametric forward-fitting” model, the observed X-ray emission of a source is fitted with the synchrotron continuum originating from a given (assumed) shape of the electron energy distribution, instead of the assumed spectral form of the non-thermal emission continuum. Therefore, the XSPEC fitting with the SYNCHROTRON model allows us to check in particular if the suppressed soft X-ray flux of HESS J1943+213 is due to the excess absorption indeed, or is rather due to the high low-energy cut-off in the underlying electron energy distribution (see in this context the case of 1ES 0229+200; Tavecchio et al. 2009; Kaufmann et al. 2011). In order to reduce the number of model free parameters, in the fitting procedure we assumed a single power-law electron energy distribution $dN/d\gamma \propto \gamma^{-s}$ with fixed energy index $s = 3.0$ and the maximum electron Lorentz factor $\gamma_{\text{max}} = 10^8 / \sqrt{\delta B' / 0.1\ \text{G}}$ (where δ is the Doppler factor of the emission region, and B' is the comoving magnetic field intensity); only the minimum

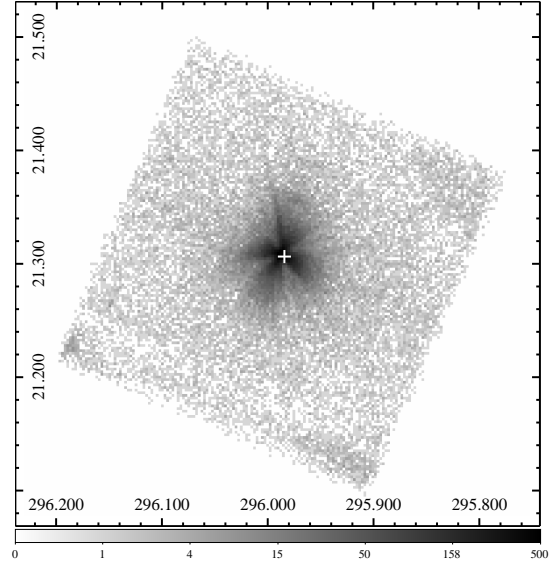


FIG. 1.— *Suzaku* XIS0+3 image of HESS J1943+213 with a pixel scale of $8.32''\ \text{pixel}^{-1}$. Horizontal and vertical axes are R.A. (J2000) and Dec. (J2000), respectively, in units of degrees. White cross denotes the source position measured by *Chandra*. The positions of the NVSS, EVN, *WISE*, and 2MASS counterparts overlap with the *Chandra* source localization, and hence are not shown here. A slight offset between the *Suzaku* and *Chandra* positions is within the $\lesssim 1\ \text{arcmin}$ *Suzaku* pointing accuracy.

electron Lorentz factor γ_{min} and the absorbing column density N_{H} were allowed to vary. The modeling returned $\gamma_{\text{min}} = 10^{5.8^{+0.02}_{-0.05}} / \sqrt{\delta B' / 0.1\ \text{G}}$, and $N_{\text{H}} = (1.23^{+0.06}_{-0.04}) \times 10^{22}\ \text{cm}^{-2}$ still in excess of the Galactic value, even though the observed flux decrease below 1 keV was in this case ascribed partly to the high low-energy electron cut-off. We note that the analogous modeling with N_{H} fixed at the Galactic value resulted in a large reduced chi-square, while on the other hand the modeling with frozen $\gamma_{\text{min}} = 10^5 / \sqrt{\delta B' / 0.1\ \text{G}}$ returned $s = 3.03^{+0.04}_{-0.05}$ and $N_{\text{H}} = (1.39 \pm 0.03) \times 10^{22}\ \text{cm}^{-2}$ in agreement with the emission continuum power-law fit discussed in the previous paragraph. Hence, we conclude that the signatures for the excess absorption in the X-ray spectrum of HESS J1943+213, even though on a rather modest level, can nonetheless be claimed robustly.

We note that previously some evidence for the intrinsic absorption of the X-ray spectra of HBLs has been presented only in a few cases, namely Mrk 501 (Kataoka et al. 1999; Abdo et al. 2011), and more recently 1RXS J101015.9–311909 (Abramowski et al. 2012).

3.2. GeV Emission of HESS J1943+213

Figure 4 shows the *Fermi*-LAT count map of the 10° radius circular region centered on HESS J1943+213 in the 10–300 GeV photon energy range. A weak GeV counterpart seems to be present at the position of HESS J1943+213 ($l = 57.764^\circ$, $b = -1.295^\circ$ in Galactic coordinates), but similar faint point-like enhancements are also seen along the Galactic plane, where the intense foreground Galactic diffuse emission dramatically dilutes any signal from γ -ray emitters located in the plane. In order to minimize the number of degrees of freedom, we tested only the hypothesis that there is a LAT source at the HESS position. We investigated the detection significance using *gtlike* following the analysis flow described in

¹⁸ <http://heasarc.gsfc.nasa.gov/cgi-bin/Tools/w3nh/w3nh.pl>

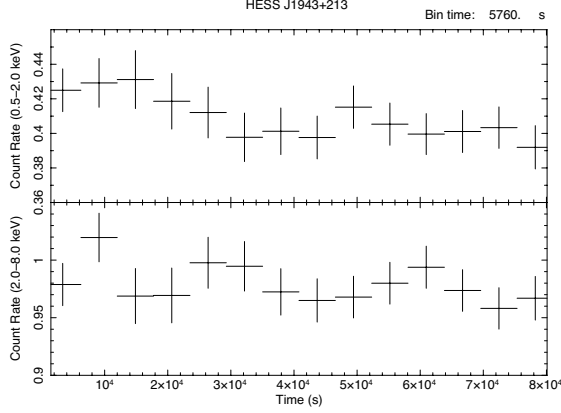


FIG. 2.— Background-subtracted *Suzaku* XIS0+3 light curve of HESS J1943+213 with 5760 s bins (Upper panel: 0.5–2.0 keV, Lower panel: 2.0–8.0 keV).

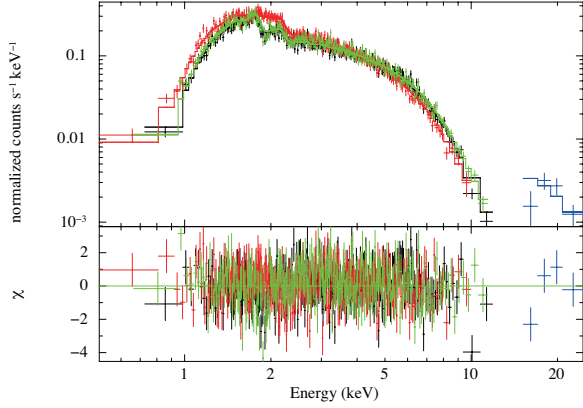


FIG. 3.— *Suzaku* spectrum of HESS J1943+213 in the 0.5–25 keV range obtained with XIS and HXD/PIN. Black, red, and green crosses denote the XIS0, XIS1, and XIS3 data, respectively, together with PIN data shown in blue. The best power-law model fit, discussed in § 3.1, is also displayed as black, red, green and blue curves.

§2.3 and obtained the Test Statistic (TS) value of 22.3, which is just below the formal detection threshold of $TS = 25$ (corresponding to a $\sim 5\sigma$ significance). Note that the TS is defined as $-2(\ln L_0 - \ln L_1)$, where L_0 and L_1 are the likelihood values with and without the source, respectively (see Mattox et al. 1996). Here we cannot exclude a possibility for the detection of a spurious source coincident with HESS J1943+213 simply due to subtraction of the imperfect template for the Galactic diffuse emission. In fact, the presence of several similar faint point-like features along the Galactic plane in Figure 4 may suggest that this is indeed the case. In addition, assuming the source detection, the derived power-law index of the 10–300 GeV counterpart of HESS J1943+213 is $\Gamma \sim 2.4$, which is suspiciously soft, although this may indicate a spectral turnover around that energy range. Analysis of newly released Pass 7 reprocessed LAT data¹⁹ accumulated over 5 years shows a detection of HESS J1943+213 with a rather flat spectrum ($\Gamma \sim 1.6$) at energies above 1 GeV (Peter et al. 2014), consistent with our suggestion of a spectral turnover at higher energies. Given all these cautions and limitations, instead of claiming the detection here we provide only

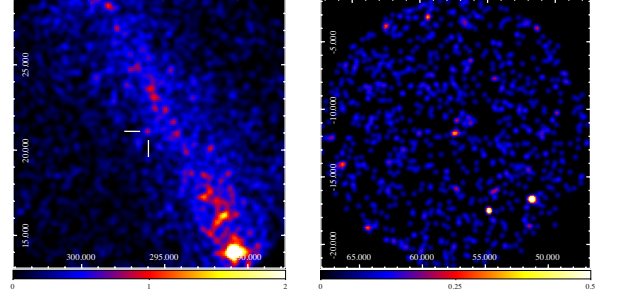


FIG. 4.— *Left*: Fermi-LAT 10–300 GeV count map centered on the position of HESS J1943+213 (R.A.=295.9792°, Dec.=21.30222°), which is indicated by white ticks. *Right*: Same as the *Left* figure but for the 10° radius circular region centered on the position of 1ES 0347–121 (R.A.=57.3466°, Dec.=−11.9908°). Both images are smoothed with Gaussian kernel of three pixels (scale: 0.1° per pixel). Note that the size of the plotted area is different between the two images (*Left* figure is more zoomed).

the 95% flux upper limits for HESS J1943+213: $F_{10-30\text{ GeV}} < 2.5 \times 10^{-12} \text{ erg cm}^{-2} \text{ s}^{-1}$, $F_{30-100\text{ GeV}} < 4.1 \times 10^{-12} \text{ erg cm}^{-2} \text{ s}^{-1}$, and $F_{100-300\text{ GeV}} < 2.7 \times 10^{-12} \text{ erg cm}^{-2} \text{ s}^{-1}$, assuming single power-law spectra with photon indices $\Gamma = 2.0$ in each band and using at the point that the $-\log(\text{likelihood})$ increased by 1.36. These are shown in the SED representation in Figure 5, along with the H.E.S.S. spectrum from Abramowski et al. (2011), the infrared (*WISE* and *UKIDSS*) data discussed in § 2.1.4, and finally all the available (archival and the new *Suzaku*) X-ray spectra of the source introduced and analyzed in § 2.1.2 and 3.1.

3.3. GeV Emission of 1ES 0347–121

In contrast, the only known extreme HBL that was missing thus far its GeV counterpart, 1ES 0347–121, is now clearly detected in the most recent accumulation of the *Fermi*-LAT data. We derived $TS = 51.0$ and power-law index $\Gamma_{\text{LAT}} = 1.65 \pm 0.17$ with the 1–300 GeV flux of $(3.0 \pm 0.7) \times 10^{-10} \text{ ph cm}^{-2} \text{ s}^{-1}$ for the source. The rather low GeV flux of the source precluded any variability studies. The broad-band SED of the blazar is given in Figure 5, including the newly derived LAT data points, the H.E.S.S. spectrum from Aharonian et al. (2007b), and optical to X-ray data introduced and discussed in § 2.2.

4. DISCUSSION

The broad-band SEDs of HESS J1943+213 and 1ES 0347–121 shown in Figure 5 resemble each other closely, although some differences can be noted as well. In particular, the X-ray continuum of 1ES 0347–121, which is known to vary (see Tavecchio et al. 2011), is in general steeper than that of HESS J1943+213. Also, the IR segments of the spectra are distinct, although this difference seems to be consistent with the idea of a more prominent contribution from the elliptical host in HESS J1943+213 due to the smaller distance of the source ($\sim 600 \text{ Mpc}$ versus $\simeq 900 \text{ Mpc}$ for 1ES 0347–121; see the discussion below). The overall correspondence between the two spectra strongly supports the blazar scenario for HESS J1943+213.

4.1. Possible identification of HESS J1943+213

The nature of HESS J1943+213 is puzzling and the subject of ongoing debate. Three main scenarios identifying the source as a HMXB, a young PWN, or an extreme HBL have

¹⁹ available at <http://fermi.gsfc.nasa.gov/cgi-bin/ssc/LAT/LATDataQuery.cgi>

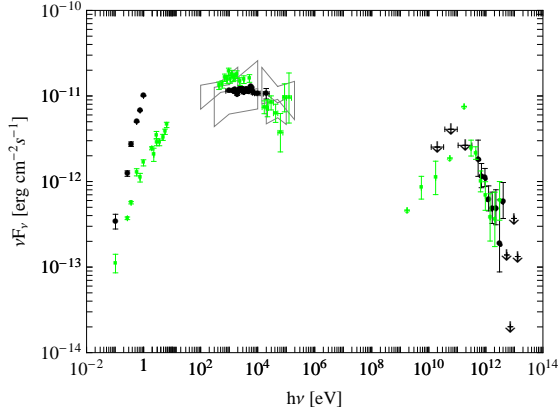


FIG. 5.— Broad-band SEDs of HESS J1943+213 and 1ES 0347-121. Black circles and large arrows correspond to the HESS J1943+213 VHE fluxes/upper limits taken from Abramowski et al. (2011), as well as the *WISE*, *UKIDSS*, *Suzaku* (re-binned XIS0+PIN), and *Fermi*-LAT data derived in this paper; gray bowties denote the archival X-ray spectra of the source (see § 2.1 and 3.2). Green squares and small arrows correspond to the 1ES 0347-121 VHE, *Swift*-UVOT & XRT, and ATOM (host galaxy-subtracted) data taken from Aharonian et al. (2007b), the updated *Swift*-BAT spectrum from Baumgartner et al. (2013), along with the *Fermi*-LAT, *WISE*, and the 2MASS fluxes derived in this paper (see § 2.2 and 3.3).

been outlined in Abramowski et al. (2011) and discussed later in Leahy & Tian (2012) and Gabányi et al. (2013). Here we briefly revisit this issue in light of the new data.

The flat X-ray spectrum of HESS J1943+213 with photon index $\Gamma_X = 2.0$ and no high-energy cut-off up to the 100 keV range, together with the very soft VHE spectrum $\Gamma_{\text{VHE}} = 3.2 \pm 0.5$, are consistent with the HMXB hypothesis. The lack of any orbital modulation in the X-ray band might be baffling in this context, but still does not exclude the possibility of the discussed object being a binary system. Similarly, no (or a very weak) GeV counterpart does not contradict the idea (keeping in mind the case of HESS J0632+057; see Caliendo et al. 2013). The most problematic aspect of the scenario is, however, the absence of a massive companion manifesting as a pronounce IR/optical source. As discussed in Abramowski et al. (2011), the 2MASS *K*-band counterpart of HESS J1943+213 could in principle be attributed to the massive O or Be-type star taking into account the 2MASS and *Swift*-UVOT upper limits derived at shorter wavelengths, but only in the case of a large distance to the system, $d \simeq 25$ kpc. This would in turn imply exceptionally high (for an HMXB) X-ray luminosity, exceeding $10^{36} \text{ erg s}^{-1}$. In addition, the arcmin-scale elongated radio halo of HESS J1943+213 discovered by Gabányi et al. (2013) would be similarly in conflict with the binary scenario. The analysis of the *Suzaku* data presented in this paper does not add any new conclusive piece of evidence to the above discussion, as no orbital modulation has been detected in our new X-ray exposure. However, the *WISE* and especially *UKIDSS* detections of the infrared counterpart of HESS J1943+213 discussed in this paper, with the resulting fluxes below the previous upper limits, would push the distance of the presumed O-type stellar companion of the high-energy source even outside the 25 kpc radius, making the HMXB hypothesis even less plausible.

In the framework of the PWN model, no extension of the source in the H.E.S.S. data together with the VHE/X-ray luminosity ratio $L_{1-30\text{TeV}}/L_{2-10\text{keV}} \simeq 0.04$ would imply a young age ($\simeq 10^3$ yr) and a relatively high, Crab-like spin-down

power ($\dot{E} \simeq 10^{38} \text{ erg s}^{-1}$) of the system located within 16 kpc (Abramowski et al. 2011). On the other hand, the soft VHE spectrum and the point-like appearance of the source in the *Chandra* data question to some extent the PWN nature of HESS J1943+213. In addition, based on the H I absorption spectrum, Leahy & Tian (2012) argued for the source distance exceeding 16 kpc. These objections have been addressed by Gabányi et al. (2013) who, based on the newly acquired EVN and archival VLA data, argued that the discussed object can still be a PWN left over after a supernova explosion that happened in a low-density environment at the distance of $d \simeq 17$ kpc. The fact that the X-ray counterpart of HESS J1943+213 appears point-like for *Suzaku*-XIS and unresolved even by *Chandra* is not any strong argument against the PWN hypothesis. However, the presence of a bright flat-spectrum mid- to near-infrared counterpart, as discussed in this paper, is unexpected for a PWN.

A comparison of high-energy spectral properties between HESS J1943+213 and bona fide extreme HBLs is summarized in Table 1 and discussed in more detail in the next section by means of a spectral model comparison with 1ES 0347-121. This comparison indicates that the multi-wavelength spectral properties of HESS J1943+213 are in principle consistent with it being a member of this class, even taking into account the hard, broad-band X-ray continuum and a very weak GeV emission of the source. The amorphous arcmin-scale radio halo surrounding the target (Gabányi et al. 2013) would fit this interpretation as well, since the previous VLA studies revealed the presence of analogous features in several BL Lacs (e.g., Ulvestad & Johnston 1984; Ulvestad & Antonucci 1986). The lack of X-ray variability implied by different X-ray pointings spread over several years, including our new *Suzaku* observations as well as the continuous *Swift*-BAT monitoring, may however cast doubt on the blazar identification. In addition, Gabányi et al. (2013) noted that the brightness temperature of the HESS J1943+213 radio core, $T_b \sim 8 \times 10^7$ K, is much lower than those typically measured in radio cores of blazars, and BL Lacs in particular. While the steady X-ray emission of the target could be explained by a particular duty cycle of HBLs, which seem to be able to undergo extended periods of quiescence (see in this context, e.g., Kaufmann et al. 2011; Perri et al. 2007, for 1ES 0229+200 and PKS 0548-322, respectively), the relatively low radio brightness temperature — if intrinsic to the source instead of being due to a small-angular size scattering cloud on the line-of-sight within the Galaxy (see the discussion in Gabányi et al. 2013) — may indeed be considered as problematic for the blazar hypothesis. We however note in this context that, on the other hand, no superluminal velocities have been found in the TeV-bright HBLs on milli-arcsec scales, despite several dedicated observational programs (e.g., Piner et al. 2010, and references therein), and yet such apparent superluminal velocities are considered to be one of the hallmark properties of blazars in general. Note also that in a recent systematic ~ 1 milli-arcsecond resolution survey of radio-faint BL Lacs (Liuzzo et al. 2013) using the Very Long Baseline Array (VLBA), most are characterized by faint ~ 10 mJy radio cores with inferred brightness temperatures (see Kovalev et al. 2005, section 5.4 therein) as low as a few 10^8 K.

Finally, the newly available *WISE* and *UKIDSS* data for HESS J1943+213 are consistent with the spectrum of the expected host galaxy located at a larger distance: this is demonstrated in Figure 7, where we plotted the template of a lu-

minous elliptical placed at 600 Mpc (bolometric luminosity $L_{0.1-10\mu\text{m}} \simeq 7 \times 10^{44} \text{ erg s}^{-1}$; template taken from Silva et al. 1998). As argued below, such a distance would additionally be in accord with the overall energetics of the source in the blazar scenario.

4.2. Spectral Modeling

If HESS J1943+213 is indeed an extreme HBL, its unique properties — in particular its steady hard X-ray continuum together with very soft VHE spectrum — may be relevant in the context of constraining the IGMF intensity (Neronov & Vovk 2010; Tavecchio et al. 2011; Dermer et al. 2011). Unfortunately, the intense diffuse Galactic emission in the direction of this source hampers its high significance detection in the *Fermi*-LAT range, which is crucial for such an analysis. Extreme HBLs located at higher Galactic latitudes, such as 1ES 0347–121, could therefore be more suitable for this purpose. Hence, we first report on the spectral modeling of 1ES 0347–121 including the new *Fermi*-LAT detection reported in this paper. We then repeat the same modeling for HESS J1943+213 assuming its blazar nature, predominantly in order to access the source energetics.

In the fitting procedure we adopt a model that includes the radiation mechanisms of synchrotron and synchrotron self-Compton (SSC; for details of the model and the χ^2 minimization technique see Finke et al. 2008). Additionally, we include a cascade component, from inverse-Compton up-scattering of cosmic microwave background (CMB) photons by the electron-positron pairs created by primary TeV photons absorbed by the EBL. This component was calculated using the method described by Dermer et al. (2011), with the Finke et al. (2010) EBL model, a jet opening angle of 0.1 rad, and the IGMF coherence length of $\lambda_B = 1$ Mpc, assuming there is no significant amount of γ -rays from ultra-high energy cosmic rays interacting with the CMB and EBL (e.g., Essey & Kusenko 2010), and no significant synchrotron energy losses for the created electron-positron pairs (Broderick et al. 2012). We assume that both 1ES 0347–121 and HESS J1943+213 have been emitting VHE γ -rays at their current levels for 3 yr and ~ 1 M yr, respectively, from the jet regions characterized by the light-crossing timescale of 10^5 s.

The resulting model curves of 1ES 0347–121 for different values of the IGMF between $B_{\text{IG}} = 10^{-16}$ G and 10^{-19} G are shown in Figure 6. The corresponding model parameters are listed in Table 2. Note that the comoving size of the emission blob R'_b is calculated from a given variability timescale t_{var} (model parameter) as $R'_b = c\delta t_{\text{var}}/(1+z)$, where c is the speed of light, δ is the beaming factor of the jet, and z is the redshift of the source. Also, the electron distribution is assumed to be of a broken power-law form, with low- and high-energy photon indices denoted as s_1 and s_2 , respectively. The best fit, as determined using the reduced χ^2 statistic, is formally provided by the model with $B_{\text{IG}} = 10^{-16}$ G, for which the cascade is minimized. Any higher B_{IG} would give an identical fit due to a negligible cascade contribution. Given the model and all the caveats and assumptions that go into it, it seems therefore likely that $B_{\text{IG}} \gtrsim 3 \times 10^{-17}$ G. If λ_B is lower than the assumed 1 Mpc, the resulting constraint on the IGMF would be stronger, since $B_{\text{IG}} \propto \lambda_B^{-1/2}$. If, however, $\lambda_B > 1$ Mpc, the constraint would be essentially unchanged, since in this case the electrons lose basically all of their energy within one correlation length (e.g., Neronov & Semikoz 2009). Our lower limit is about two orders of magnitude be-

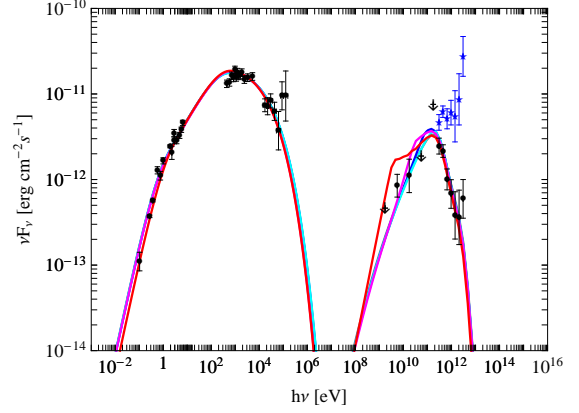


FIG. 6.— Broadband SED of 1ES 0347–121. Black filled circles/arrows correspond to the same data as shown in Figure 5 (see also § 2.2 and 3.3). Blue stars denote the H.E.S.S. fluxes of the source corrected for the EBL absorption using the model of Finke et al. (2010). The model curves included in the figure represent the sum of all the considered emission components (synchrotron, SSC, and cascade), for different values of the IGMF, namely $B_{\text{IG}} = 10^{-16}$ G (gray), $B_{\text{IG}} = 10^{-17.5}$ G (blue), $B_{\text{IG}} = 10^{-17}$ G (cyan), $B_{\text{IG}} = 10^{-18}$ G (magenta), and $B_{\text{IG}} = 10^{-19}$ G (red; see § 4.2 for the model fit description).

low that derived by Tavecchio et al. (2011). The reason for this is that Tavecchio et al. assumed that the γ -ray emission of 1ES 0347–121 is stable over 10^7 year, while in our case 3 yr is assumed. We note that, if the engine timescale is longer (say 10 or 1000 yr instead of 3 yr as we assumed here, there will be more cascade emission, and the IGMF has to be larger to keep the cascade below the LAT emission for 1ES 0347–121. Therefore, the assumption of a short engine timescale is more conservative, since it provides a weaker constraint on the IGMF. Future high-sensitivity observations in the TeV range using Cherenkov Telescope Array, for example, would provide much tighter constraints on this crucial variability timescale. On the other hand, extremely low *jet* magnetic field and high minimum electron Lorentz factor, both of which were claimed for the source by Tavecchio et al. (2011), are confirmed in our modeling (see Table 2).

In the modeling of HESS J1943+213 (see Figure 7), we assumed the electron energy distribution in a single power-law form with index $s = 3$ between electron Lorentz factors $\gamma_{\text{min}} = 10^5$ and $\gamma_{\text{max}} = 3 \times 10^7$ (in agreement with the SYNCHROTRON modeling presented in § 3.1). The model parameters are tabulated in Table 3. The fit — characterized by the reduced $\chi^2/\text{dof} = 5.8/6$ based on the SSC match to the H.E.S.S. data only — returns the jet Doppler factor $\delta = 70$ (the maximum value from the assumed range of this model parameter) and the emission region magnetic field $B = 0.78$ mG, which are both consistent with the analogous values derived for the other extreme HBLs (Tavecchio et al. 2010). The corresponding total jet kinetic luminosity carried by the radiating electrons is $P_{j,e} \simeq 6.3 \times 10^{44} \text{ erg s}^{-1}$. The calculated cascade spectra are as expected considerably below the newly derived *Fermi*-LAT upper limits (as long as the IGM is not orders of magnitudes lower than 10^{-18} G).

5. CONCLUSION

Based on the new *Suzaku* and *Fermi*-LAT data, augmented by the infrared photometry from the *WISE* and *UKIDSS* surveys, here we argue that the ‘extreme HBL’ scenario for HESS J1943+213 remains the most plausible option. Our

TABLE 1
HIGH-ENERGY SPECTRAL PROPERTIES OF EXTREME HBLs.

Name	z	$\Gamma_{\text{VHE}} \pm \text{stat} \pm \text{sys}$	Γ_{LAT}	Quiescent X-ray spectrum [†]
HESS J1943+213	?	$3.10 \pm 0.12 \pm 0.12$	—	$\Gamma = 2.0$ with excess absorption
1ES 0229+200	0.140	$2.50 \pm 0.19 \pm 0.10$	1.36 ± 0.25	$\Gamma = 1.84 \pm 0.02$ with excess absorption
1ES 0347–121	0.185	$3.10 \pm 0.23 \pm 0.10$	1.65 ± 0.17	$\Gamma = 1.82 \pm 0.03$ with excess absorption
1ES 1101–232	0.186	2.94 ± 0.20	1.80 ± 0.31	$\Gamma_{\text{low}} = 2.04 \pm 0.02$, $\Gamma_{\text{high}} = 2.32 \pm 0.02$, $E_{\text{brk}} = 1.37 \pm 0.08$ keV
1ES 1218+304	0.182	3.07 ± 0.09	1.63 ± 0.12	$\Gamma = 2.51 \pm 0.05$ with excess absorption
RGB J0710+591	0.125	$2.69 \pm 0.26 \pm 0.20$	1.46 ± 0.22	$\Gamma = 1.86 \pm 0.01$ with Galactic absorption
1ES 0414+009	0.287	$3.5 \pm 0.3 \pm 0.2$	1.9 ± 0.1	$\Gamma = 2.4 \pm 0.1$ with excess absorption
H 2356–309	0.165	$3.06 \pm 0.15 \pm 0.10$	1.89 ± 0.17	$\Gamma_{\text{low}} = 2.08 \pm 0.03$, $\Gamma_{\text{high}} = 2.32 \pm 0.02$, $E_{\text{brk}} = 1.00 \pm 0.08$ keV

NOTE. — [†] Spectral information in lowest X-ray flux is taken from literature.

NOTE. — Spectral information for the lowest X-ray flux is taken from the literature. References: HESS J1943+213 (Abramowski et al. 2011), and this work. 1ES 0229+200 (Aharonian et al. 2007d; Vovk et al. 2012; Kaufmann et al. 2011). 1ES 0347–121 (Aharonian et al. 2007b; Perlman et al. 2005), and this work. 1ES 1101–232 (Aharonian et al. 2007a; Ackermann et al. 2011a; Reimer et al. 2008). 1ES 1218+304 (Acciari et al. 2010a; Donato et al. 2005). RGB J0710+591 (Acciari et al. 2010b). 1ES 0414+009 (Aliu et al. 2012). H 2356–309 (H.E.S.S. Collaboration et al. 2010; Ackermann et al. 2011b).

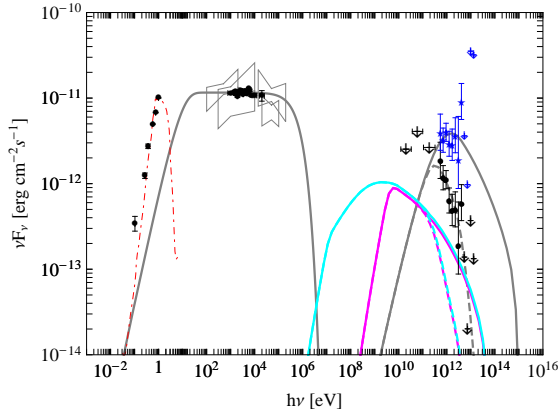


FIG. 7.— Broadband SED of HESS J1943+213. Black filled circles/large arrows correspond to the same data as shown in Figure 5 (see also § 2.1 and 3.2). Blue stars and small arrows denote the de-absorbed VHE spectrum, assuming a source distance of 600 Mpc and the EBL model of Finke et al. (2010). Various model curves represent different emission components calculated in the framework of the ‘extreme HBL fit’ (see § 4.2), including synchrotron and SSC ones (gray curves), along with the cascade spectra calculated for $B_{\text{IG}} = 10^{-16}$ G (magenta curves) and $B_{\text{IG}} = 10^{-18}$ G (cyan curves); the dashed curves denote the spectra with the EBL attenuation included; thin red dot-dashed curve illustrates the starlight of a giant elliptical galaxy located at a distance of 600 Mpc.

conclusion follows from (i) the derived best-quality X-ray spectrum of the source revealing excess absorption, (ii) the fact that the combined *WISE* and *UKIDSS* spectrum of the infrared counterpart of the source is consistent with a luminous elliptical host located at the distance of ~ 600 Mpc, (iii) the broad-band spectral fitting returning the model parameters in agreement with the analogous ones claimed for the established extreme HBLs, and also (iv) a close resemblance between the broad-band SEDs of HESS J1943+213 and other extreme HBLs, in particular 1ES 0347–121. In addition, lack of any GeV counterpart of HESS J1943+213 in the *Fermi*-LAT data, but on the other hand a presence of arcmin-scale radio halo, can then be easily understood as well. Yet the persistent hard X-ray emission together with particularly low brightness temperature of the radio core seem to be at odds, at least to some extent, with the blazar nature of the source.

Here we also report on the detection of 1ES 0347–121 in the most recent accumulation of the *Fermi*-LAT data, noting that this object was the only known extreme HBL missing thus far its GeV counterpart. The newly derived GeV spectrum of the source, along with the updated hard X-ray and infrared fluxes, enabled detailed broad-band modeling including the cascade component due to the electron-positron pairs created by the EBL-absorbed TeV jet emission. We confirm the extremely low jet magnetic field and high minimum electron Lorentz factor reported by Tavecchio et al. (2011). However, our model fits yield more conservative lower limits for the IGMF intensity ($\gtrsim 3 \times 10^{-17}$ G) than those derived previously by Tavecchio et al. (2011).

Y.T.T is supported by Kakenhi 24840031. Ł.S. was supported by Polish NSC grant DEC-2012/04/A/ST9/00083. Work by C.C.C. at NRL is supported in part by NASA DPR S-15633-Y.

The *Fermi* LAT Collaboration acknowledges generous ongoing support from a number of agencies and institutes that have supported both the development and the operation of the LAT as well as scientific data analysis. These include the National Aeronautics and Space Administration and the Department of Energy in the United States, the Commissariat à l’Energie Atomique and the Centre National de la Recherche Scientifique/Institut National de Physique Nucléaire et de Physique des Particules in France, the Agenzia Spaziale Italiana and the Istituto Nazionale di Fisica Nucleare in Italy, the Ministry of Education, Culture, Sports, Science and Technology (MEXT), High Energy Accelerator Research Organization (KEK) and Japan Aerospace Exploration Agency (JAXA) in Japan, and the K. A. Wallenberg Foundation, the Swedish Research Council and the Swedish National Space Board in Sweden.

Additional support for science analysis during the operations phase is gratefully acknowledged from the Istituto Nazionale di Astrofisica in Italy and the Centre National d’Études Spatiales in France.

REFERENCES

TABLE 2
MODEL PARAMETERS FOR THE SED OF 1ES 0347–121 SHOWN IN FIGURE 6.

Parameter	Symbol	Values				
Intergalactic Magnetic Field [G]	B_{IG}	10^{-19}	10^{-18}	3×10^{-18}	10^{-17}	10^{-16}
Reduced χ^2	χ^2/dof	17/7	9.6/7	10/7	11/7	9.5/7
Bulk Lorentz Factor	Γ	49	62	61	62	61
Doppler Factor	δ_D	49	62	61	62	61
Blazar Magnetic Field [mG]	B	3.1	1.3	1.4	1.3	1.3
Variability Timescale [s]	t_v	1×10^5	1×10^5	1×10^5	1×10^5	1×10^5
Comoving radius of blob [cm]	R'_b	1.2×10^{17}	1.6×10^{17}	1.5×10^{17}	1.6×10^{17}	1.6×10^{17}
Low-Energy Electron Spectral Index	s_1	2.0	2.0	2.0	2.0	2.0
High-Energy Electron Spectral Index	s_2	2.8	2.8	2.8	2.8	2.8
Minimum Electron Lorentz Factor	γ'_{min}	2.0×10^4	2.0×10^4	2.0×10^4	2.0×10^4	2.0×10^4
Break Electron Lorentz Factor	γ'_{brk}	4.3×10^5	6.0×10^5	5.2×10^5	5.2×10^5	5.4×10^5
Maximum Electron Lorentz Factor	γ'_{max}	2.3×10^6	3.1×10^6	3.4×10^6	3.5×10^6	3.5×10^6
Jet Power in Magnetic Field [erg s $^{-1}$]	$P_{j,B}$	2.6×10^{42}	1.3×10^{42}	1.3×10^{42}	1.3×10^{42}	1.2×10^{42}
Jet Power in Electrons [erg s $^{-1}$]	$P_{j,e}$	5.1×10^{44}	1.0×10^{45}	1.0×10^{45}	1.1×10^{45}	1.1×10^{45}

TABLE 3
MODEL PARAMETERS FOR THE SED OF HESS J1943+213 SHOWN IN FIGURE 7.

Parameter	Symbol	Values	
Intergalactic Magnetic Field [G]	B_{IG}	10^{-18}	10^{-16}
Reduced χ^2	χ^2/dof	5.7/7	5.7/7
Bulk Lorentz Factor	Γ	70	70
Doppler Factor	δ_D	70	70
Blazar Magnetic Field [mG]	B	0.78	0.78
Variability Timescale [s]	t_v	1×10^5	1×10^5
Comoving radius of blob [cm]	R'_b	1.9×10^{17}	1.9×10^{17}
Low-Energy Electron Spectral Index	p_1	3.0	3.0
Minimum Electron Lorentz Factor	γ'_{min}	1.0×10^5	1.0×10^5
Maximum Electron Lorentz Factor	γ'_{max}	3.0×10^7	3.0×10^7
Jet Power in Magnetic Field [erg s $^{-1}$]	$P_{j,B}$	7.8×10^{41}	7.8×10^{41}
Jet Power in Electrons [erg s $^{-1}$]	$P_{j,e}$	6.3×10^{44}	6.3×10^{44}

- . 2012, A&A, 542, A94
Acciari, V. A., et al. 2010a, ApJ, 709, L163
—. 2010b, ApJ, 715, L49
Ackermann, M., et al. 2011a, ApJ, 743, 171
—. 2011b, ApJ, 743, 171
Aharonian, F., et al. 2005, Science, 307, 1938
—. 2007a, A&A, 470, 475
—. 2007b, A&A, 473, L25
—. 2007d, A&A, 475, L9
Aliu, E., et al. 2012, ApJ, 755, 118
Atwood, W. B., et al. 2009, ApJ, 697, 1071
Baumgartner, W. H., Tueller, J., Markwardt, C. B., Skinner, G. K., Barthelmy, S., Mushotzky, R. F., Evans, P. A., & Gehrels, N. 2013, ApJS, 207, 19
Bouchet, L., Jourdain, E., Roques, J.-P., Strong, A., Diehl, R., Lebrun, F., & Terrier, R. 2008, ApJ, 679, 1315
Broderick, A. E., Chang, P., & Pfrommer, C. 2012, ApJ, 752, 22
Caliandro, G. A., et al. 2013, MNRAS
Costamante, L., et al. 2001, A&A, 371, 512
Cusumano, G., et al. 2010, A&A, 510, A48
D’Avezac, P., Dubus, G., & Giebels, B. 2007, A&A, 469, 857
Dermer, C. D., Cavadini, M., Razzaque, S., Finke, J. D., Chiang, J., & Lott, B. 2011, ApJ, 733, L21
Donato, D., Sambruna, R. M., & Gliozzi, M. 2005, A&A, 433, 1163
Essey, W., & Kusenko, A. 2010, Astroparticle Physics, 33, 81
Finke, J. D. 2013, ApJ, 763, 134
Finke, J. D., Dermer, C. D., & Böttcher, M. 2008, ApJ, 686, 181
Finke, J. D., Razzaque, S., & Dermer, C. D. 2010, ApJ, 712, 238
Fossati, G., Maraschi, L., Celotti, A., Comastri, A., & Ghisellini, G. 1998, MNRAS, 299, 433
Gabányi, K. É., Dubner, G., Giacani, E., Paragi, Z., Frey, S., & Pidopryhora, Y. 2013, ApJ, 762, 63
Ghisellini, G., Celotti, A., Fossati, G., Maraschi, L., & Comastri, A. 1998, MNRAS, 301, 451
Ghisellini, G., & Tavecchio, F. 2008, MNRAS, 387, 1669
Giommi, P., Padovani, P., & Polenta, G. 2013, MNRAS, 431, 1914
Giommi, P., Padovani, P., Polenta, G., Turriziani, S., D’Elia, V., & Piranomonte, S. 2012, MNRAS, 420, 2899
H.E.S.S. Collaboration et al. 2010, A&A, 516, A56
Kalberla, P. M. W., Burton, W. B., Hartmann, D., Arnal, E. M., Bajaja, E., Morras, R., & Pöppel, W. G. L. 2005, A&A, 440, 775
Kataoka, J., et al. 1999, ApJ, 514, 138
Kaufmann, S., Wagner, S. J., Tibolla, O., & Hauser, M. 2011, A&A, 534, A130
Kokubun, M., et al. 2007, PASJ, 59, 53
Koyama, K., et al. 2007, PASJ, 59, 23
Kovalev, Y. Y., Kellermann, K. I., Lister, M. L., et al. 2005, AJ, 130, 2473
Landi, R., et al. 2009, A&A, 493, 893
Leahy, D. A., & Tian, W. W. 2012, A&A, 539, A128
Liuzzo, E., et al. 2013, A&A, 560, A23
Lucas, P. W., et al. 2008, MNRAS, 391, 136
Mattox, J. R., et al. 1996, ApJ, 461, 396
Mitsuda, K., et al. 2007, PASJ, 59, 1
Neronov, A., & Semikoz, D. V. 2009, Phys. Rev. D, 80, 123012
Neronov, A., & Vovk, I. 2010, Science, 328, 73
Nolan, P. L., et al. 2012, ApJS, 199, 31
Perlmutter, E. S., et al. 2005, ApJ, 625, 727
Perri, M., et al. 2007, A&A, 462, 889
Peter, D., et al. submitted to A&A
Piner, B. G., Pant, N., & Edwards, P. G. 2010, ApJ, 723, 1150
Reimer, A., Costamante, L., Madejski, G., Reimer, O., & Dorner, D. 2008, ApJ, 682, 775
Schlegel, D. J., Finkbeiner, D. P., & Davis, M. 1998, ApJ, 500, 525
Silva, L., Granato, G. L., Bressan, A., & Danese, L. 1998, ApJ, 509, 103
Takahashi, T., et al. 2007, PASJ, 59, 35
Tavecchio, F., Ghisellini, G., Bonnoli, G., & Foschini, L. 2011, MNRAS, 414, 3566
Tavecchio, F., Ghisellini, G., Ghirlanda, G., Costamante, L., & Franceschini, A. 2009, MNRAS, 399, L59
Tavecchio, F., Ghisellini, G., Ghirlanda, G., Foschini, L., & Maraschi, L. 2010, MNRAS, 401, 1570
Tomsick, J. A., Chaty, S., Rodriguez, J., Walter, R., & Kaaret, P. 2009, ApJ, 701, 811

Tundo, E., Moretti, A., Tozzi, P., Teng, L., Rosati, P., Tagliaferri, G., & Campana, S. 2012, *A&A*, 547, A57
Ulvestad, J. S., & Antonucci, R. R. J. 1986, *AJ*, 92, 6
Ulvestad, J. S., & Johnston, K. J. 1984, *AJ*, 89, 189

Ushio, M., et al. 2009, *ApJ*, 699, 1964
—. 2010, *ApJ*, 724, 1509
Vovk, I., Taylor, A. M., Semikoz, D., & Neronov, A. 2012, *ApJ*, 747, L14
Wright, E. L., et al. 2010, *AJ*, 140, 1868